

# O STAR X-RAY LINE PROFILES EXPLAINED BY RADIATION TRANSFER IN INHOMOGENEOUS STELLAR WIND

L. M. Oskinova, A. Feldmeier, and W.-R. Hamann

Universität Potsdam, Astrophysik, 14469 Potsdam, Germany

## ABSTRACT

It is commonly adopted that X-rays from O stars are produced deep inside the stellar wind, and transported outwards through the bulk of the expanding matter which attenuates the radiation and affects the shape of emission line profiles. The ability of Chandra and XMM-Newton to resolve these lines spectroscopically provided a stringent test for the theory of X-ray production. It turned out that none of the existing models was able to reproduce the observations consistently. The major caveat of these models was the underlying assumption of a smooth stellar wind. Motivated by the various observational evidence that the stellar winds are in fact structured, we present a 2-D model of a stochastic, inhomogeneous wind. The X-ray radiative transfer is derived for such media. It is shown that profiles from a clumped wind differ drastically from those predicted by conventional homogeneous models. We review the up-to-date observations of X-ray line profiles from stellar winds and present line fits obtained from the inhomogeneous wind model. The necessity to account for inhomogeneities in calculating the X-ray transport in massive star winds, including for HMXB is highlighted.

Key words: X-rays; massive stars; stellar winds.

## 1. CLUMPED WINDS FROM O-TYPE STARS

Young and massive O-type stars possess strong stellar winds. The winds are fast, with typical velocities up to 2500 km/s, and dense, with mass-loss rates  $\dot{M} \sim 10^{-7} M_{\odot}/\text{yr}$ . The driving mechanism for the mass-loss from OB stars has been identified with radiation pressure on spectral lines. A corresponding theory was developed by Castor et al. (1975). After consequent improvements, this theory correctly predicts the observed mass-loss rates and wind velocities (Pauldrach et al., 1986). However, it was pointed out early (Lucy & Solomon, 1970), and later further investigated (Owocki & Rybicki, 1984), that the stationary solution for a line-driven wind

is unstable; small perturbation grow quickly and result in strong shocks. The most detailed hydrodynamic modeling of the line driven instability was presented by Feldmeier et al. (1997). These calculations show that the winds are strongly inhomogeneous with large density, velocity and temperature variations. The density inhomogeneity is commonly referred to as wind clumping. Runacres & Owocki (2005) studied the 1-D evolution of instability-generated structures in the winds. They have demonstrated that the winds are essentially clumped out to distances of  $1000 R_{*}$ .

The theoretical prediction of the wind clumping is confirmed observationally. Bouret et al. (2005) conducted a quantitative analysis of the far-ultraviolet spectrum of two Galactic O stars using the last generation NLTE stellar atmosphere codes. Their study provided a strong evidence of wind clumping in O stars. It was pointed out that accounting for wind clumping is essential when determining the wind properties of O stars.

One of the most significant consequences of the clumping is the reduction of empirically derived mass-loss rates by at least a factor of 3 (Hamann & Koesterke, 1998; Bouret et al., 2005). The stellar mass-loss rate determines the wind density, and therefore the wind opacity. Studying the effects of absorption in the observed X-ray spectra allows to probe the wind opacity. Analysis of the X-ray emission from individual stellar winds in the O stars  $\delta$  Ori (Miller et al., 2002) and  $\zeta$  Pup (Kramer et al., 2003) have shown that the attenuation by the stellar wind is significantly smaller than expected from standard homogeneous wind models.

Similar conclusions are reached from the analysis of X-rays from colliding wind binaries (CWB). Such systems consist of two massive early type stars, where each component has a strong wind. The copious X-ray emission is produced in the zone where the stellar winds collide. At certain orbital phases the X-rays formed in the colliding wind zone travel towards an observer through the bulk of the stellar wind of one companion. Deriving the absorbing column density from X-ray spectroscopy constrains the wind density. Mass-loss rates can be inferred and compared with the models. An analysis of XMM-

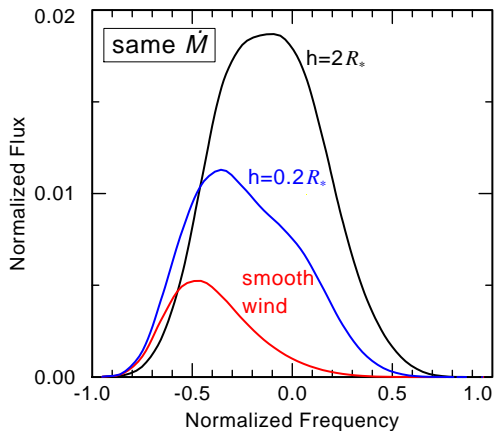


Figure 1. Comparison between example line profiles emerging from a clumped and a smooth wind of the same mass-loss rate, velocity law ( $\beta = 1.5$ ), and equal X-ray emissivity. Frequency is measured relative to the line center and in Doppler units referring to the terminal wind velocity  $v_\infty$ . The average separation between clumps  $h$  is indicated.

Newton observations of the massive binary  $\gamma^2$  Vel was presented by Schild et al. (2004). They deduced the column density of absorbing material from fits of the X-ray spectra and showed that the observed attenuation of X-rays is much weaker than expected from smooth stellar wind models. To reconcile theory with observations, Schild et al. (2004) suggest that the ratio of clump density to smooth wind density has to be high, and the volume filling factor of the clumps has to be small. Significantly, similar conclusions were reached from Chandra and RXTE observations of WR 140 (Pollock et al., 2005). Alike  $\gamma^2$  Vel, the column density expected from the stellar atmosphere models that account for the clumping in first approximation only, is a factor of four higher than the column density inferred from the X-ray spectrum analysis.

Spectacular evidence of wind clumping comes from X-ray spectroscopy of high-mass X-ray binaries (HMXB). In some of these systems a neutron star (NS) is on a close orbit deeply inside the stellar wind of the massive star. The X-ray emission with a power law spectrum is produced as a result of Bondi-Hoyle accretion of the stellar wind onto the NS. These X-rays photoionize the stellar wind. The resulting X-ray spectrum shows a large variety of emission features, including lines from H-like and He-like ions and a number of fluorescent emission lines. Sako et al. (2003) reviewed spectroscopic results obtained by X-ray observatories for several wind-fed HMXBs. They conclude that the observed spectra can be explained only as originating in a clumped stellar wind where cool dense blobs are embedded in rarefied photoionized gas. Van der Meer et al. (2005) studied stochastic variability of the X-ray light curve in 4U 1700-37 and its X-ray spectra. They shown that the feeding of the NS by a strongly clumped stellar wind is consistent with the observed temporal and spectral vari-

ability.

X-ray emission is also intrinsic for clumped stellar winds of single stars. Feldmeier et al. (1997) performed hydrodynamic simulations of an O star wind. They showed that the de-shadowing instability leads to strong gas compression resulting in dense cool shell fragments. The space between fragments is essentially void, but at the outer side of the dense shells exist extended gas reservoirs. Small gas cloudlets are ablated from these reservoirs, and accelerated to high speed by radiation pressure. Propagating through an almost perfect vacuum, they catch up with the next outer shell and ram into it. In this collision, the gas parcels are heated and emit thermal X-rays. The X-ray emission ceases when the wind reaches its terminal speed. In contrast, the cool fragments are maintained out to large distances, despite their expansion due to the internal pressure. Thus there are two disjunctive structural wind components – hot gas parcels that emit X-rays and highly compressed cool fragments that attenuate this radiation.

## 2. TRANSFER OF X-RAYS IN A CLUMPED STELLAR WIND

Wind inhomogeneity alters the radiative transfer significantly. We have studied the effects of wind fragmentation on X-ray line formation analytically in the limit of infinitely many stochastically distributed fragments (Feldmeier et al., 2003), and numerically for more realistic stellar winds (Oskinova et al., 2004). The latter work describes the model and the code used in the present paper to reproduce the observed X-ray emission line profiles. It is assumed that X-rays are emitted by a large number of stochastically distributed hot gas parcels within the wind acceleration zone. These gas parcels are permeated with the numerous aligned cool shell fragments (i.e. clumps). The fragments are also distributed stochastically and propagate, maintaining their solid angle, outwards with  $v(r)$ . They persist till large distances from the stellar surface.

Because the average stellar mass-loss rate is constant, the mass confined within each clump is, on average, the total mass of the stellar wind divided by the number of shell fragments. The mass-loss rate  $\dot{M}$  is fixed for a specific star from UV/optical spectral analysis. We employ the average number density of the fragments,  $n(r)$ , as a free parameter. The fragments are radially compressed and therefore aligned. Thus the optical depth,  $\tau_{\text{sh}}(E, \vartheta_{\text{sh}})$ , of each individual shell fragment depends on its mass, the mass absorption coefficient at energy  $E$ , and the intersection angle between the shell and the line of sight ( $\vartheta_{\text{sh}}$ ).

The fate of each X-ray photon emitted deep inside the wind and propagating outwards depends on whether it escapes from the wind without encountering any shell fragment, or it accidentally hits a fragment. The chance to hit a shell is smaller when the average separation between

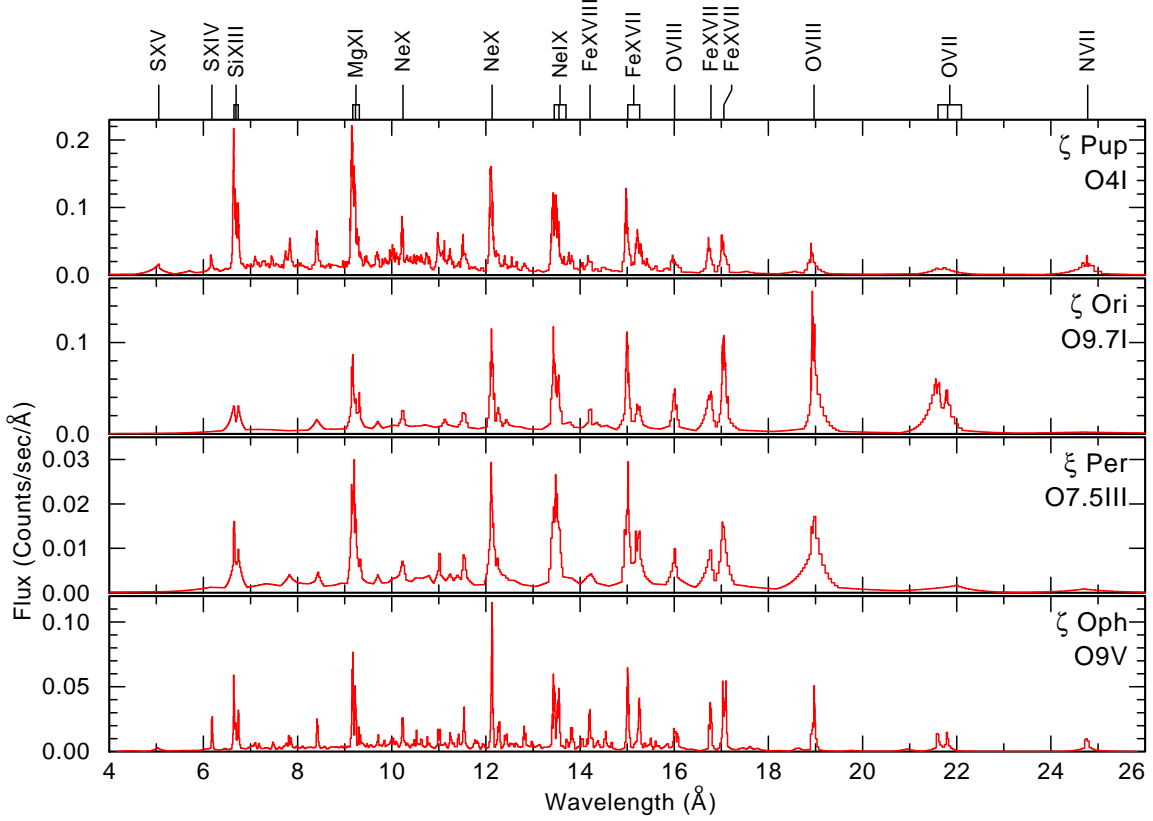


Figure 2. De-reddened HETGS spectra of prominent O stars. All stars except  $\zeta$  Ori are evolved runaway stars, as reflected by the enhanced N/O ratio.

shells,  $h$ , is larger. The average separation  $h$  depends on the number density of the fragments and their cross-section:  $h = \langle n(r)\sigma \rangle^{-1}$ .

The probability that the photon that has hit a shell is absorbed is  $1 - \exp(-\tau_{\text{sh}})$ . Therefore the *effective opacity*  $\bar{\tau}$  in the stellar wind depends on the number density of shells  $n(r)$ , the cross section of the shells  $\sigma$ , and the probability of a photon to be absorbed in a shell. The optical depth along a photon path through the clumpy wind is

$$\bar{\tau} = \int n(r) \sigma (1 - e^{-\tau_{\text{sh}}(E)}) dr \quad (1)$$

Importantly, in the limit of a very large number of fragments, Eq. (1) recovers the formula for the optical depth in a smooth wind (Oskinova et al., 2004).

Assume now that radiation of intensity  $I_0$  is emitted somewhere in the wind. After passing through the wind this intensity will be reduced to

$$I = I_0 e^{-\bar{\tau}} \quad (2)$$

From Eqs. (1, 2) one can see that for optically thick clumps ( $\tau_{\text{sh}} \gg 1$ ) the effective optical depth  $\bar{\tau}$  is independent of the energy. The opacity in the clumped wind is effectively grey.

Our modeling shows that the wind fragmentation drastically reduces the opacity of the wind. Therefore X-rays

produced deep inside the wind can effectively escape, which would be totally absorbed in a homogeneous wind of the same mass-loss rate. A comparison between predicted line profiles emerging from clumped and smooth winds of the same mass-loss rate is shown in Fig. 1.

The line width is determined by the velocity field of the hot plasma. It is commonly accepted to approximate the velocity field in the stellar wind by a “ $\beta$ -law” of the form

$$v(r) = v_\infty \left(1 - \frac{1}{r}\right)^\beta, \quad (3)$$

where the distance  $r$  is normalized to the stellar radius. The terminal velocity  $v_\infty$  is deduced by analyzing UV/optical spectra. Hence, the free parameter to describe the width of an X-ray line is  $\beta$ .

Intrinsic line intensity  $I_0$  can be calculated from hydrodynamic wind models but it is not done yet. To compare the model and the observed line profiles we normalize the flux in the model line to the observed one. Thus only two free parameters are required to fit the observed line: the average separation between clumps  $h$ , which defines the attenuation; and  $\beta$ , which defines the line broadening.

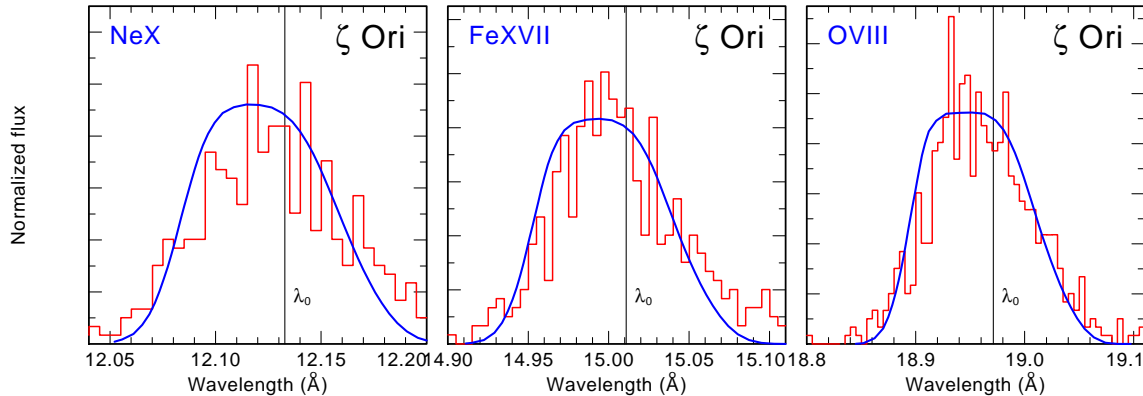


Figure 3. Thin lines: co-added  $meg\pm 1$  lines observed in the spectrum of  $\zeta$  Ori. Thick lines: model line profiles. The rest wavelength corrected for the stellar radial velocity is indicated by  $\lambda_0$ . Model line profiles are calculated using  $h \approx 1 R_*$ ,  $\beta = 3$  and the appropriate for this star  $\dot{M}$  and  $v_\infty$ .

Table 1. Stellar wind parameters from Repolust et al. (2004) and Lamers et al. (2001)

Name	$v_\infty$ [km/s]	$\dot{M}$ [ $M_\odot \text{yr}^{-1}$ ]
$\zeta$ Pup	2250	$9.0 \times 10^{-6}$
$\zeta$ Ori	2100	$2.5 \times 10^{-6}$
$\xi$ Per	2450	$1.8 \times 10^{-6}$
$\zeta$ Oph	1550	$\leq 1.8 \times 10^{-7}$

### 3. GRATING OBSERVATIONS OF O STARS

We have selected Chandra HETGS observations of prominent O stars to fit the observed line profiles in the framework of a clumped wind model. The de-reddened spectra of selected stars are shown in Figure 2. We have chosen three stars that are most likely single, and therefore their X-ray emission can be solely attributed to the stellar wind itself. The probability of a massive star being single is significantly higher among runaway stars and three stars in our sample are runaway stars that have not shown indications of binarity. The fourth star,  $\zeta$  Ori, is a known binary. We include  $\zeta$  Ori in the sample because the initial interpretation of the observed emission lines from this star caused doubts in the validity of the shock model of X-ray production (Waldron & Cassinelli, 2001). The wind parameters of the stars are listed in Table 1.

The observed spectra in the 4 – 24 Å band were fitted using the *xspec* package. The spectrum of  $\zeta$  Pup has the highest S/N. A satisfactory spectral fit for this star can be achieved only by using a model that accounts for the continuum emission as well as for the lines. The *apec* model is capable to reproduce the X-ray emission lines in the  $\zeta$  Pup spectrum. The continuum can be fitted by thermal bremsstrahlung. Importantly, the temperatures obtained from the emission lines and from the continuum are identical,  $kT_X \approx 0.6$  keV, and in good agreement with

the predictions of the wind shock model.

The plasma in hot star winds is not expected to be isothermal. However, the strong shock condition implies that the maximum temperature of the shock material scales with the square of the preshock wind velocity. Constraining the temperature of hot gas in  $\zeta$  Oph provides an interesting test, because this star has the slowest stellar wind. It is expected that its X-ray plasma temperature should be a factor of two lower than in  $\zeta$  Pup. To estimate temperatures we used H-like to He-like ion line ratios of Mg and Si. Our estimates show that the temperature in  $\zeta$  Oph is indeed lower than in  $\zeta$  Pup. A temperature less than 0.4 keV is also consistent with the results of fitting the  $\zeta$  Oph spectrum with *xspec*.

The strongest emission lines observed in the spectra of our sample stars are shown in Figs. 3, 4, 5 and 6. Lines in all spectra are broad, blueshifted and symmetric. The Ne X line is a doublet ( $\lambda_{01,02} = 12.132, 12.138$  Å). Kramer et al. (2003) provided a detailed analysis of emission lines in  $\zeta$  Pup using the smooth wind model. They concluded that the lines are broadened to the terminal wind velocity and have similar shapes across the spectrum.

### 4. MODEL FITTING OF OBSERVED LINES

A detailed modeling of the X-ray spectra and emission line profiles can be done only by means of full stellar atmosphere models. Conventional “standard” models, e.g. *apec*, strictly speaking are not adequate for the fast moving stellar winds, and cannot predict expected line profiles. The approach of Kramer et al. (2003) was to normalize the model line flux to the observed one. The line profile fitting was used to constrain the wind optical depth at the line wavelength. This is possible because in the smooth wind approximation, the shape of emission line is sensitive to the amount of material on the line of sight. The more skewed the line is, the more opaque is the wind (Ignace, 2001).

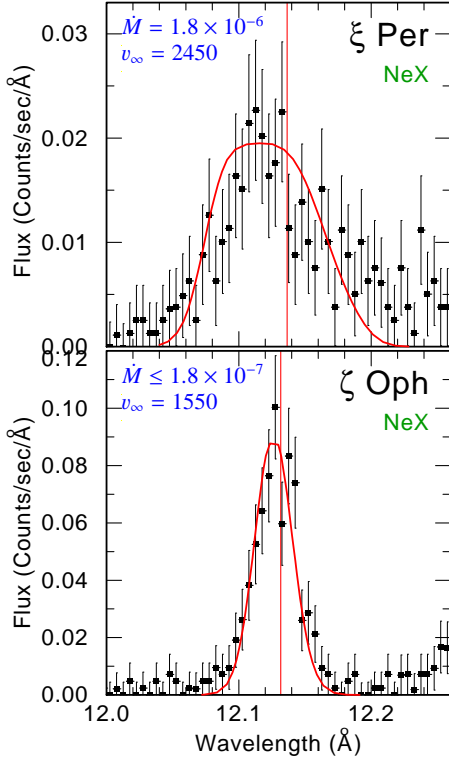


Figure 4. Observed and model NeX line in  $\xi$  Per and  $\zeta$  Oph. Model line profiles are calculated using  $h \approx 1 R_*$  and  $\beta = 3$  for both stars.  $\dot{M}$  and  $v_\infty$  are from Table 1.

This does not hold in a clumped wind. The shape of an emission line is sensitive to the spatial distribution of the clumps in the winds. When a large number of clumps is effectively black, the radiation can still escape between them. Thus the average separation between clumps is the key parameter determining how much X-ray radiation escapes. When clumps are compressed in radial direction, the line profile is distinctly symmetric although its maximum is blueshifted as can be seen in Fig. 1. When the separation between clumps is small, the wind is nearly homogeneous and emergent emission lines have skewed shapes characteristic for a smooth wind. However, if the separation between clumps is large enough, the lines shape becomes symmetric. Therefore, the average clump separation can be constrained by fitting the observed line profiles. Shown in Fig. 3 are the lines observed in the spectrum of  $\zeta$  Ori. As can be seen, the observed lines are broad, symmetric and blueshifted. The lines are very well reproduced by our fragmented wind model. Line profiles resolved by Chandra in the spectra of  $\xi$  Per and  $\zeta$  Oph and model fits for these lines are shown in Figs. 4 and 5. All model fits are produced assuming that the average separation between the shell fragments is of the order of the stellar radius.

The distance from the stellar core where X-ray emission originates can be estimated from line ratios of He-like ions. The strong UV field of an O star causes radiative de-population of metastable  $^3S$  level, weakening forbidden (F) line in favor of the recombination (I) line

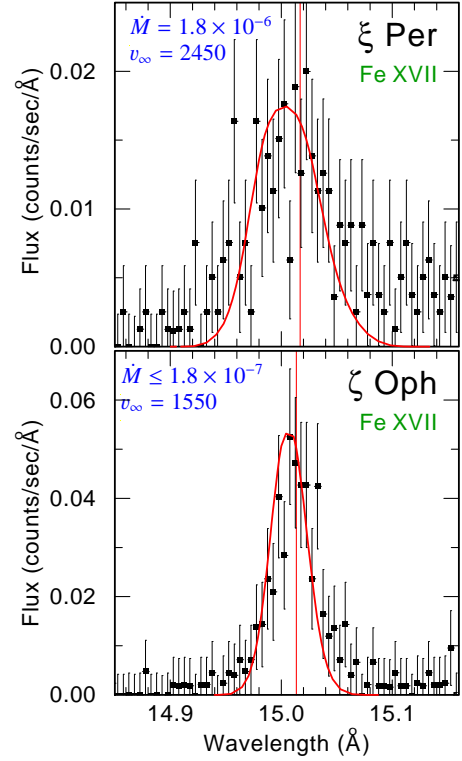


Figure 5. Observed and modeled Fe XVII line in  $\xi$  Per and  $\zeta$  Oph. Model parameters the same as in Fig. 4.

(Porquet et al., 2001). Therefore ratio F/I is a diagnostic of UV field. The UV field dilutes with radius, thus the ratio F/I provides information about the distance from the stellar photosphere. The values of F/I obtained for different ions are similar. For instance, our analysis of Mg XI and Si XIII in  $\zeta$  Oph indicates that the plasma is located between 1.8 and 6  $R_*$  from the stellar core.

When the location of the hot plasma is constrained and the terminal velocity of the wind is known, parameter  $\beta$  can be varied to adjust the model line width. As can be seen in Figs. 4 and 5, the width of lines differs significantly between stars. Lines observed in  $\xi$  Per, the star with the fastest wind, are much broader than the lines in  $\zeta$  Oph, where the stellar wind is slowest.

The model lines shown in Figs. 3, 4 and 5 required rather large values of  $\beta \geq 2$ , indicating slow wind acceleration. This  $\beta$  is much higher than the usual  $\beta \approx 0.8$  inferred from analyses of UV/optical spectra and predicted from theoretical wind models (Repolust et al., 2004). The lines in the  $\zeta$  Pup spectrum, fitted with smaller values of  $\beta = 1.5$ , are shown in Fig. 6.

## 5. WIND CLUMPING IN HMXBS

The effects of wind clumping are important for the interpretation of the X-ray spectra from the wind-fed HMXBs. Spectra obtained at orbital phases near X-ray eclipse are

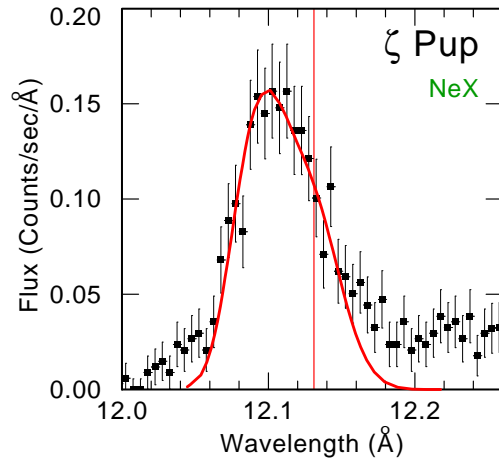


Figure 6. Observed and model Ne X line in  $\zeta$  Pup. Model line profile is calculated using  $h \approx 0.2 R_*$ ,  $\beta = 1.5$  and the appropriate for this star  $M$  and  $v_\infty$ .

dominated by emission reprocessed in the stellar wind. The X-rays from the accretion onto the compact object are scattered in the wind. The Compton optical depth scales with density, and the effects of clumping should be included in the modeling of the scattering in the wind. In addition, an emission line spectrum is emerging from the photoionized stellar wind near the compact object. On their way to the observer, X-rays are attenuated in the stellar wind. Clumping reduces the absorption and makes it less wavelength dependent.

Clumping also affects the size of the photoionized region. Its radius is determined by the balance of ionization and recombination. The ionization rate scales with density, but the recombination rate scales with density squared. Therefore, if the wind consists of numerous but optically thin clumps, the radius of the photoionized region would be reduced compared to a homogeneous wind. If, however, the wind is compressed in a relatively small number of optically thick clumps, then the photoionized region becomes more extended compared to the smooth wind case (but with recombined clumps embedded). Hence, the radius of the photoionized region is determined by the clump filling factor and the density of the clumps.

## 6. CONCLUSIONS

There are firm observational evidences of stellar winds being strongly inhomogeneous.

Clumping strongly reduces the opacity of the stellar wind for the X-ray emission.

Absorption in a clumped wind is effectively independent of wavelength.

The line profiles observed in X-ray spectra of O stars are broad, symmetric and blueshifted.

O star X-ray line profiles are explained by radiation transfer in an inhomogeneous stellar wind.

## REFERENCES

- Bouret J.-C., Lanz T., Hillier D.J. 2005, *A&A*, 438, 301
- Castor J.I., Abbott D.C., Klein R.I. 1975, *ApJ*, 195, 157
- Feldmeier A., Puls J., Pauldrach A.W.A. 1997, *A&A*, 322, 878
- Feldmeier A., Oskinova L., Hamann W.-R. 2003, *A&A*, 403, 217
- Ignace R. 2001, *ApJ*, 549, L119
- Hamann W.-R. & Koesterke L. 1998, *A&A*, 335, 1003
- Kramer R.H., Cohen D.H., Owock S.P. 2003, *ApJ*, 592, 532
- Lamers H.J.G.L.M., Haser S., de Koter A., Leitherer C. 1999, *ApJ*, 516, 872
- Lucy L.B. & Solomon P.M. 1970, *ApJ*, 159, 879
- Miller N.A., Cassinelli J.P., Waldron W.L., MacFarlane J.J., Cohen D.H. 2002, *ApJ*, 577, 951
- Oskinova L.M., Feldmeier A., Hamann W.-R. 2004 *A&A*422, 675
- Owocki S.P. & Rybicki G.B. 1984, *ApJ*, 284, 337
- Pauldrach A., Puls J., Kudritzki R.P. 1986, *A&A*, 164, 86
- Pollock A.M.T., Corcoran M.F., Stevens I.R., Williams P.M. 2005, *ApJ*, 629, 482
- Porquet D., Mewe R., Dubau J., Raassen A.J.J., Kaastra J.S. 2001, *A&A*, 376, 1113
- Repolust T., Puls J., Herrero A. 2004, *A&A*, 415, 349
- Runacres M.C. & Owocki S.P. 2005, *A&A*, 429, 323
- Sako M., Kahn S.M., Paerels F., Liedahl D.A., Watanabe S., Nagase F., & Takahashi T., 2003, in *High Resolution X-ray Spectroscopy with XMM-Newton and Chandra*, ed. G. Branduardi-Raymont (astro-ph/p309503)
- Schild H., Güdel M., Mewe R., et al. 2004, *A&A*, 422, 177
- van der Meer A., Kaper L., Di Salvo T., et al. 2005, *A&A*, 432, 999
- Waldron W.L. & Cassinelli J.P. 2001, *ApJ*, 548, L45